Lithium isotope evidence for enhanced hydrological cycling during Oceanic Anoxic Event 2

Philip A.E. Pogge von Strandmann[1*], Hugh C. Jenkyns[1] and Richard G. Woodfine[1†]

[1]Department of Earth Sciences, University of Oxford, South Parks Road, Oxford, OX1 3AN, UK

*Contact email: philipvs@earth.ox.ac.uk

[†]Current address: BP, Chertsey Road, Sudbury-on-Thames, UK

Contains:

- Methods (Supplementary Figures 1 and 2, Supplementary Table 1)
- Results (Supplementary Tables 2–4)
- Models (Supplementary Figures 3–8, Supplementary Tables 5 and 6)
- Li isotope fractionation factors in calcite
- Supplementary References

Methods

Carbonate leaching

Approximately 200 mg of bulk carbonate were leached in 0.1M HCl for 1 hour. This level of acid dilution was utilised in order to avoid gaining Li from the silicate clays that are in the marls, given the high [Li] and relatively low δ^7Li in these minerals. Analyses of clays remaining after leaching from Eastbourne yield δ^7Li = -2.5±4.5‰ (2sd, n = 4), with an average Al/Ca~0.04 mol/mol. Mass balance calculations show that Al/Ca in carbonates must be >0.8 mmol/mol before carbonate with δ^7Li=20‰ is measurably (>0.5‰) perturbed by Li leached from clays. This supposition is also borne out by leaching experiments of a sample of the Plenus Marl from the Chalk at Eastbourne (Fig. S1).

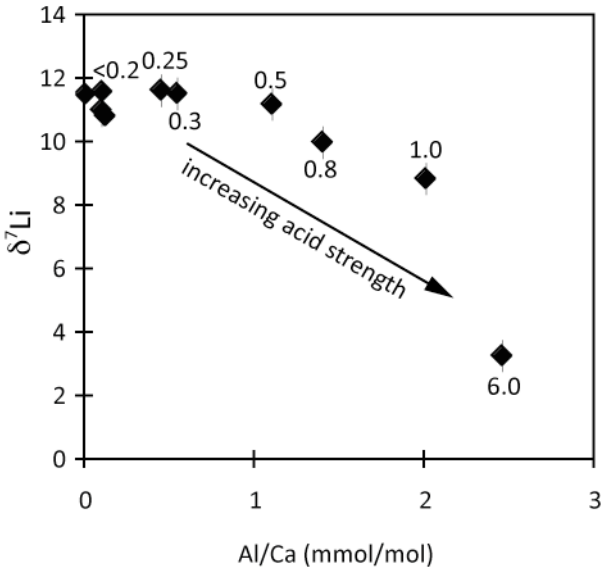

Figure S1. Results of continuously stronger acid leaches on a sample of the Plenus Marl, showing the increasing effect of clay-derived Li. The numbers next to the data points reflect the molarity of HCl used.

This experiment was continued by performing a Tessier sequential extraction[51]. By this method, the exchangeable fraction and the carbonate fraction of sediment can be

selectively removed and analysed. Hence the exchangeable fraction of two carbonate samples was removed with 1M NaOAc, and subsequently the carbonate fraction was leached with 1M NaOAc adjusted to pH5 with acetic acid[51]. The addition of significant Na-salts to the sample by this method means that it would be difficult to perform for all samples, because of the risk of overloading the column chemistry. However, selective leaching of a few samples can show whether the weak-acid leaches are reliable. The results show that little Li (<10%) is associated with the exchangeable fraction, which is any case is isotopically similar to the carbonate fraction. The isotope results of the selectively leached carbonate are within analytical uncertainty of bulk sample leached with dilute acid (Table S1).

	δ^7Li (‰)	2s.d.
PM300		
exchangeable	6.0	0.4
carbonate	6.2	1.0
bulk	5.9	0.4
PM620		
exchangeable	5.9	0.6
carbonate	9.8	0.7
bulk	10.2	0.4

Table S1. Results of selective Tessier leaching of two carbonate samples.

Sr/Ca and Mn/Ca ratios were also measured in each carbonate leach. While Sr and Mn abundances will indicate the leaching of silicates, they also have the disadvantage that their abundance in carbonate will vary across the OAE, due to changes in weathering and, for Mn, depositional redox conditions. However, it is still possible to compare our results with those of other studies. In particular, Sr/Ca and Mn/Ca have been published from different samples of the Eastbourne section[52]. Sr/Ca from both studies agree well, and Mn/Ca ratios from this study are slightly lower than

those reported by[52], with carbonate-associated ratios (i.e., corrected for the silicate component) from the latter study <1.7 mmol/mol during the OAE, and <1.17 in this study. Again, these values strongly suggest that silicate clays are not contributing significant Li to our carbonate values.

The detailed work performed on Eastbourne allows other checks to ascertain whether the Li isotope ratios reported in this study were affected by Li leached from clays. In general, if low δ^7Li in carbonates reflects high chemical weathering intensities and weathering rates (see main text), it is possible that a high clay content in the Chalk will correspond to low chalk δ^7Li, because both may be compounded by higher weathering. However, Pearce et al. (2009) measured $CaCO_3$ content of different samples from the Eastbourne Chalk, which can be used as a tracer of clay contents. The two data sets were precisely aligned using C isotope stratigraphy (Fig. S2), and show that, although the initial δ^7Li minimum correlates with a period of high clay content, the second δ^7Li decrease correlates with relatively low clay contents and, further, that there are intervals with a high clay proportion that show no corresponding δ^7Li change. Hence, we maintain that the Li isotope variations reported in this study are not due to leaching of variable clay contents in the carbonates.

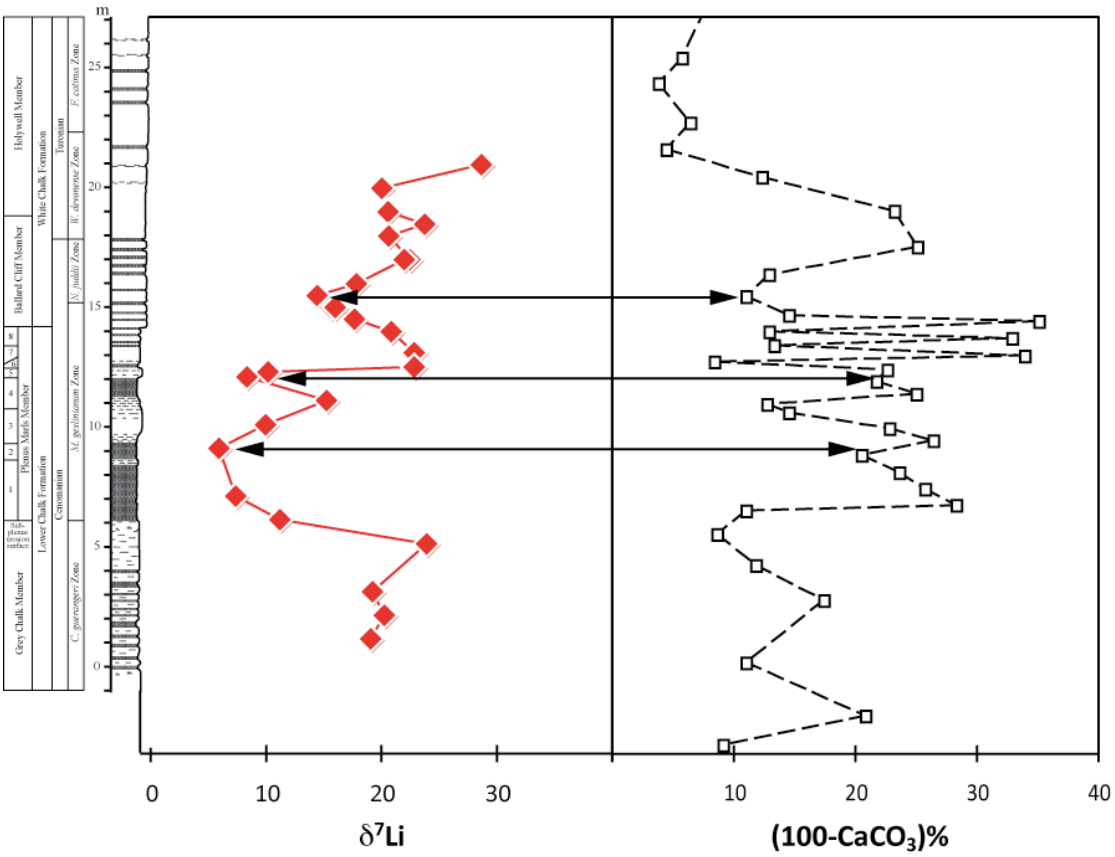

Fig. S2. Li isotope data and stratigraphy from this study compared to rock composition data (% of rock that is not carbonate) from the Eastbourne section given by Pearce et al. (2009)[52]. The arrows join stratigraphic levels where δ^7Li is low. It is clear that low δ^7Li does not correspond solely to high clay contents, and that high clay contents also do not correspond to low δ^7Li.

Chemistry and analyses

A split of each solution was retained for cation analysis using an Elan Quadrupole ICP-MS (inductively coupled plasma mass spectrometer). Samples were matrix matched to 10μg/g Ca and calibrated against a set of synthetic standards made up from single element solutions. Accuracy and precision were assessed by repeated analyses of seawater, the international reference material JLs-1 and, in order to assess reproducibility of both analyses and carbonate leaching, repeated dissolutions and

analysis of a sample of the Plenus Marl from Eastbourne were undertaken. Sample reproducibility of Li/Ca and Al/Ca was ~7% (2sd, n=6).

The larger part of each sample (typically containing 5–10ng Li) was purified by passing it through a two-stage cation-exchange procedure, as described elsewhere[53]. Given that Li isotopes fractionate during cation chromatography, it is critical to have column yields close to 100%[54]. To assess the efficacy of this process, splits of the solution were collected before and after the collected bracket for Li, and were analysed for Li content. Results showed that <0.1% of Li was present in these splits.

The total procedural blank for Li isotope analysis is ~0.02ng Li, which is insignificant compared to the mass of sample used. Analyses were performed on a Nu Plasma HR multi-collector ICP-MS, using a sample-standard bracketing system relative to the LSVEC standard[55]. Each sample was measured three separate times during an analytical session, repeat measurements being separated by several hours, but during the same analytical session. Each individual measurement consisted of 10 ratios (10s total integration time), giving a total integration time of 300 s/sample. At an uptake rate of 75 μl/min, the sensitivity for a 20 ng/ml solution is ~18 pA of ^{7}Li. Background instrumental Li intensity, typically ~0.01pA, was subtracted from each measurement. Accuracy and external reproducibility, as assessed from seawater, is 31.1±0.6‰ (2sd, n=16, chemistry=16). Precision was also assessed from repeated analyses (including leaching and chemistry) of our in-house marl standard, which also gives a reproducibility of ±0.6‰ (n=7).

Sr isotope methods

Sr isotope measurements on limestones from Raia del Pedale were performed in 1999-2002. Samples were cleaned, then crushed, and then leached in ~0.6M HCl to avoid contamination from clays. The samples were then purified in cation exchange chemistry (AG-50W X12), using 3M HCl as an eluent. The purified samples were loaded onto single outgassed Ta filaments, and analysed on a VG Isomass 54E Thermal Ionisation Mass Spectrometer (TIMS). Sr isotope ratios were normalised to a NIST SRM-987 value of 0.710250.

Results

The Li isotope measurements and Li/Ca, Al/Ca, Sr/Ca and Mn/Ca data of the carbonates are shown in Tables S2, S3 and S4.

Sample name	Height (cm)	δ^7Li (‰)	2s.d.	Li/Ca (μmol/mol)	Al/Ca (mmol/mol)	Sr/Ca (mmol/mol)	Mn/Ca (mmol/mol)
WC7.0	2090	28.7	0.3	4.4	0.3	0.51	0.49
WC6.0	1990	20.1	0.4	4.8	0.0	0.73	0.20
WC5.0	1890	20.6	0.3	3.7	b.d.l.	0.58	0.39
WC600	1840	23.8	0.6	4.4	b.d.l.	0.64	0.32
WC4.0	1790	20.7	0.6	6.0	0.1	0.58	0.82
WC3.0	1690	22.5	0.3	6.2	0.1	0.53	1.11
WC450	1690	22.0	0.4	6.0	b.d.l.	0.69	0.86
WC2.0	1590	17.8	0.2	3.8	0.2	0.57	1.04
WC300	1540	14.5	0.6	7.5	0.0	0.72	0.60
WC1.0	1490	15.7	0.5	4.3	0.1	0.59	0.62
WC250	1490	16.0	0.5	5.9	0.0	0.66	0.67
WC200	1440	17.7	0.7	6.8	0.0	0.63	0.76
WC0.0	1390	20.9	0.2	8.9	0.2	0.59	1.08
WC60	1300	22.8	0.2	10.5	b.d.l.	1.02	1.17
PM640	1240	22.8	0.4	9.2	0.0	0.97	0.89
PM620	1220	10.2	0.4	14.1	0.0	1.21	0.87
PM600	1200	8.3	0.5	22.8	0.0	1.09	0.65
PM500	1100	15.3	0.4	11.4	b.d.l.	1.35	0.61
PM400	1000	9.9	0.6	13.1	0.3	1.22	0.56
PM300	900	5.9	0.4	19.6	b.d.l.	1.24	0.60
PM100	700	7.4	0.7	17.9	0.6	1.07	0.65
GC00	600	11.2	0.5	11.3	b.d.l.	1.05	0.36
GC100	500	23.9	0.1	6.6	b.d.l.	1.28	0.29
GC300	300	19.2	0.9	7.1	b.d.l.	1.02	0.40
GC400	200	20.3	0.2	14.7	0.0	0.83	0.39
GC500	100	19.1	0.6	7.5	b.d.l.	0.82	0.26

Table S2. Data from the Eastbourne section. Note sample repeats with different sample names (as taken from different sampling trips). B.d.l. = below detection limits.

Sample name	Height (cm)	δ^7Li (‰)	2s.d.	Li/Ca (μmol/mol)	Al/Ca (mmol/mol)	Sr/Ca (mmol/mol)	Mn/Ca (mmol/mol)
SF-70	-70	23.1	0.2	1.10	0.15	0.65	0.99
SF-65	-65	27.8	0.7	2.60	b.d.l.	0.73	1.01
SF-55	-55	24.5	0.6	1.13	0.06	0.69	0.84
SF-35	-35	22.9	0.8	1.10	0.03	0.73	0.92
SF-15	-15	22.2	0.4	5.60	0.04	0.69	0.86
SF-10	-10	13.8	0.4	9.80	0.17	0.60	0.81
SF-5	-5	12.9	0.1	11.40	0.17	0.63	0.68
SF0	0	7.5	0.1	16.27	0.41	0.69	0.58
SF+10	10	5.6	0.7	19.90	0.21	0.71	0.49
SF+10b	10	6.5	0.6	19.98	0.43	0.69	0.57
SF+15	15	6.1	0.3	15.18	0.21	0.66	0.75
SF+25	25	9.9	0.7	13.17	0.17	0.61	1.06
SF+30	30	8.2	0.6	16.43	0.17	0.60	1.14
SF+45	45	15.5	0.7	4.35	0.10	0.59	1.00
SF+55	55	19.6	0.7	3.16	0.15	0.57	1.00
SF+85	85	21.4	0.4	8.74	0.11	0.57	0.86
SF+100	100	20.6	0.1	1.50	0.10	0.50	0.74
SF+150	150	23.3	0.7	2.81	b.d.l.	0.48	0.99
SF+200	200	25.1	0.5	2.03	b.d.l.	0.46	0.73

Table S3. Data from the South Ferriby section

Sample name	Height (m)	$^{87}Sr/^{86}Sr$	2s.d.	$\delta^{7}Li$ (‰)	2s.d.	Li/Ca (µmol/mol)	Al/Ca (mmol/mol)	Sr/Ca (mmol/mol)	Mn/Ca (mmol/mol)
RDP2	2			20.1	1.0	1.66	b.d.l.	0.25	0.03
RDP18	18			20.5	0.2	1.03	0.11	0.28	0.05
RDP19	19	0.70751	0.00002						
RDP21	21	0.70748	0.000021						
RDP23	23	0.70749	0.000016						
RDP25	25	0.7075	0.00002						
RDP27	27	0.70756	0.000021						
RDP27.25	27.25			18.9	1.2	0.93	b.d.l.	0.16	0.08
RDP33	33	0.70743	0.000019						
RDP37	37	0.70751	0.000019						
RDP39	39	0.70748	0.00002						
RDP41	41	0.70745	0.000021						
RDP43	43	0.70747	0.000017						
RDP44.75	44.75			16.5	1.0	2.23	b.d.l.	0.22	0.01
RDP45	45	0.70748	0.00002						
RDP47	47	0.70744	0.000009						
RDP48	48	0.70745	0.000018						
RDP49	49	0.70747	0.000023						
RDP50	50	0.70743	0.000017	14.1	1.5	2.90	0.13	0.28	0.01
RDP50.25	50.25								
RDP52	52	0.70732	0.000017						
RDP54	54	0.70743	0.000021						
RDP55	55	0.70742	0.000014						
RDP58	58	0.70743	0.00002						
RDP59	59	0.70745	0.00002						
RDP60	60	0.70752	0.000015	10.6	0.2	2.58	b.d.l.	0.25	0.02
RDP61	61	0.70741	0.000021						
RDP66	66	0.70744	0.000021						
RDP68	68	0.70742	0.000022						
RDP69.25	69.25			11.4	0.6	1.36	0.06	0.27	0.01
RDP70	70	0.70744	0.00002						
RDP72	72	0.70745	0.000021						
RDP74	74	0.70745	0.000022						
RDP76	76	0.70741	0.000021						
RDP80	80	0.70746	0.000022						
RDP81	81			13.1	0.6	1.83	0.08	0.28	0.05
RDP88	88	0.70736	0.000017						
RDP95	95			15.3	0.4				
RDP106	106	0.70739	0.000021						
RDP108	108	0.70739	0.000021						
RDP112	112	0.70747	0.000021						
RDP118	118	0.70739	0.000019						
RDP121	121			16.6	0.1	1.12	0.03	0.26	b.d.l.
RDP124	124	0.70738	0.000021						
RDP132	132	0.70739	0.000019						
RDP136	136	0.70736	0.000021						
RDP137	137			15.9	0.7	1.87	0.12	0.29	0.02
RDP142	142	0.70736	0.00002						
RDP148	148	0.70736	0.00002						
RDP150	150	0.70738	0.000021						
RDP166	166	0.70736	0.00002						
RDP170	170	0.70741	0.000016						
RDP176	176	0.70732	0.000021						
RDP181	181	0.70738	0.000021						
RDP189	189	0.70736	0.000021						
RDP194	194			18.1	0.6	1.82	b.d.l.	0.35	0.01
RDP199	199	0.70738	0.000019						
RDP201	201	0.7073	0.000032						
RDP205	205	0.70733	0.000021						
RDP217	217	0.70741	0.000025						
RDP221	221			18.8	1.3	1.44	0.42	0.32	0.06
RDP223	223	0.70742	0.000021						
RDP233	233	0.70738	0.000021						
RDP237	237	0.70736	0.00002						
RDP240	240			18.4	1.2	1.32	b.d.l.	0.22	b.d.l.
RDP245	245	0.70739	0.000032						
RDP249	249	0.70744	0.000021						
RDP253	253	0.70741	0.000026						
RDP259	259	0.70751	0.000022						
RDP261	261	0.70746	0.000013						
RDP263	263			17.6	0.9	1.19	b.d.l.	0.11	0.03
RDP265	265	0.70748	0.000021						
RDP269	269	0.70746	0.00002						
RDP271	271	0.70758	0.000013						
RDP287	287	0.70751	0.000022						
RDP293	293	0.7075	0.000022						
RDP297	297			17.0	0.4	1.44	b.d.l.	0.08	0.08
RDP301	301	0.70743	0.000024						
RDP303	303	0.70754	0.000021						
RDP308	308			16.5	0.6	1.09	b.d.l.	0.15	0.09
RDP317	317	0.70765	0.00002						

Table S4. Data from the Raia del Pedale section.

Models

A series of dynamic box models was used to model seawater Li, Ca, Sr and Os cycles, and hence explore causes of isotopic variations in these systems. The models were constructed from the basic mass-balance equation, shown here for Li:

$$\frac{dN}{dt} = F_r + F_h - F_{sed} \qquad \text{(Eqn. S1)}$$

where N is the seawater Li reservoir, and F_x represents the input and output fluxes (r = river, h = hydrothermal, sed = sediment (combined alteration of the oceanic crust, and uptake onto marine sediments). The isotopic balance equation is then given by:

$$N\frac{dR_{SW}}{dt} = F_r(R_r - R_{SW}) + F_h(R_h - R_{SW}) - F_{sed}(R_{sed} - R_{SW}) \qquad \text{(Eqn. S2)}$$

where R_x is the isotope ratio of the various fluxes. R_{sink} is given by $\Delta_{sink} = R_{sink}\text{-}R_{SW}$, where $\Delta^7Li_{sink} = 15–16‰$[56-58]. Finally, the calculation of the sink of Li (and all other elements modelled here) from seawater is based on the assumption that partitioning into the sink is due to a constant partition coefficient k, where:

$$F_{out} = k \times N \qquad \text{(Eqn. S3)}$$

The same equations were applied to the other isotopic systems, with alterations because Sr and Os have an additional source (the diagenetic flux and aeolian dust, respectively)[59-62]:

$$\frac{dN_{Ca}}{dt} = F_r + F_h - F_{carb} \qquad \text{(Eqn. S4)}$$

$$N_{Ca}\frac{dR_{SW}}{dt} = F_r(R_r - R_{SW}) + F_h(R_h - R_{SW}) - F_{carb}(R_{carb} - R_{SW}) \qquad \text{(Eqn. S5)}$$

$$\frac{dN_{Sr}}{dt} = F_r + F_h + F_{diag} - F_{carb} \qquad \text{(Eqn. S6)}$$

$$N_{Sr}\frac{dR_{SW}}{dt} = F_r(R_r - R_{SW}) + F_h(R_h - R_{SW}) + F_{diag}(R_{diag} - R_{SW}) - F_{carb}(R_{carb} - R_{SW}) \quad \text{(Eqn. S7)}$$

$$\frac{dN_{Os}}{dt} = F_r + F_{lth} + F_{hth} + F_{dust} - F_{out} \qquad \text{(Eqn. S8)}$$

$$N_{Os}\frac{dR_{SW}}{dt} = F_r(R_r - R_{SW}) + F_{lth}(R_{lth} - R_{SW}) + F_{hth}(R_{hth} - R_{SW}) + F_{dust}(R_{dust} - R_{SW}) - F_{out}(R_{out} - R_{SW})$$

(Eqn. S9)

where for Os, lth = low-temperature hydrothermal, hth = high-temperature hydrothermal, and dust = aeolian dust.

The cosmic dust input for Os was not included in the model, as it is believed that cosmic dust will not dissolve in seawater, and in any case is unlikely to have changed its flux rate over this time period. Neither Sr nor Os isotopes are fractionated during uptake into carbonates, but Li and Ca isotopes are, so this process was also accounted for in the model. Li, Ca and Sr were modelled in 10,000-year time steps, and Os in 5000-year steps, to account for the short ocean residence time of Os. Table S5 lists the values used in the models for each system.

	pre-OAE					OAE peak (if changed from previous)				
	Li	Ca	Sr		Os	Li	Ca	Sr		Os
F river (Gmol/yr)	20	23000	33	(mol/yr)	1504					
F hydro (Gmol/yr)	9	3000	24	low-T hydro (mol/yr)	92	10.8	3600	29	low-T hydro (mol/yr)	111
				high-T hydro (mol/yr)	355				high-T hydro (mol/yr)	426
F diag (Gmol/yr)			3.4							
F dust (mol/yr)					150					
R river	12	0.6	0.711		0.8	3	0.75	0.707		0.15
R hydro	7	0.9	0.7033	low-T hydro	0.878					
				high-T hydro	0.115					
R diag			0.7084							
R dust					1.05					

Table S5. Model input parameters. Modern fluxes and isotope ratios are from[58-65]. Pre-OAE parameters were chosen to fit measured data, and also based on a reconstructed global Late Cretaceous MOR spreading rate[66]. Riverine parameters were based on the assumption that continental crust was being weathered before the OAE[60,67,68], and basaltic crust during the OAE[69-75]. See rest of supplement for discussion of changes in riverine fluxes and oceanic elemental reservoirs.

Initial hydrothermal fluxes were held to be proportional to the ridge spreading rate, as determined by the GEOCARBII model[66], and Li, Ca, Sr and Os concentrations were assumed to be in the same proportions as in the present day. Pre-OAE seawater isotope ratios were taken to be in steady state, and riverine fluxes and isotope ratios were calculated in order to match measured pre-excursion values. This exercise also requires a degree of assumption, because two independent variables (flux and isotope ratio) can be brought to bear. In other words, the model solutions are non-unique, but have been chosen to be as conservative (i.e., as close to modern values) as possible. Hence, conclusions drawn from the models represent minimum estimates.

Clearly the main changes that can perturb all four isotope systems for ~400kyr are variations in hydrothermal and/or riverine fluxes. The following diagrams show the model results for several different assumptions as to the causes of the measured variability. Figure S3 shows the isotopic response if the cause of the Li isotope

excursion were purely due to an increase in the hydrothermal flux. To explain the measured change in δ^7Li, the hydrothermal flux would have to have increased by a factor of 50 for ~200kyrs. While this pattern could also explain the Ca and Os isotope excursions, $^{87}Sr/^{86}Sr$ is driven significantly more unradiogenic than any values yet determined for Phanerozoic seawater[76]. This result also shows that the cause for the unradiogenic $^{187}Os/^{188}Os$ cannot be a large increase in the hydrothermal flux[77], because it is not consistent with the Sr record.

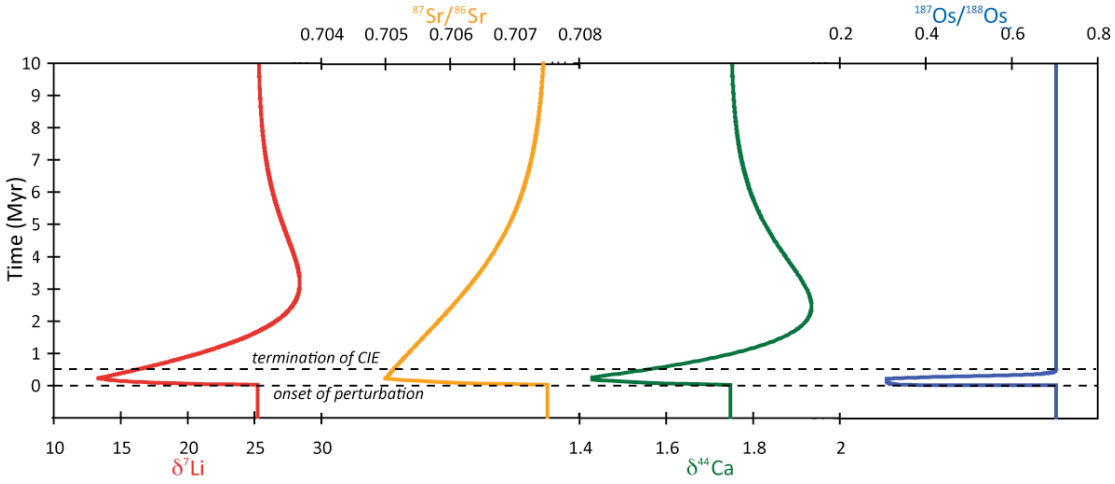

Figure S3. Effect of a 200 kyr 50× hydrothermal flux increase.

Clearly, therefore, because Sr isotopes are the most sensitive tracer of hydrothermal changes, the $^{87}Sr/^{86}Sr$ can be used to constrain the hydrothermal variability[78]. The 4 Myr trend towards more unradiogenic values[79] is taken to reflect this process, and requires a ~20% increase in the hydrothermal flux for 4 Myr. The modelled effects of this change can be seen in Fig. S4.

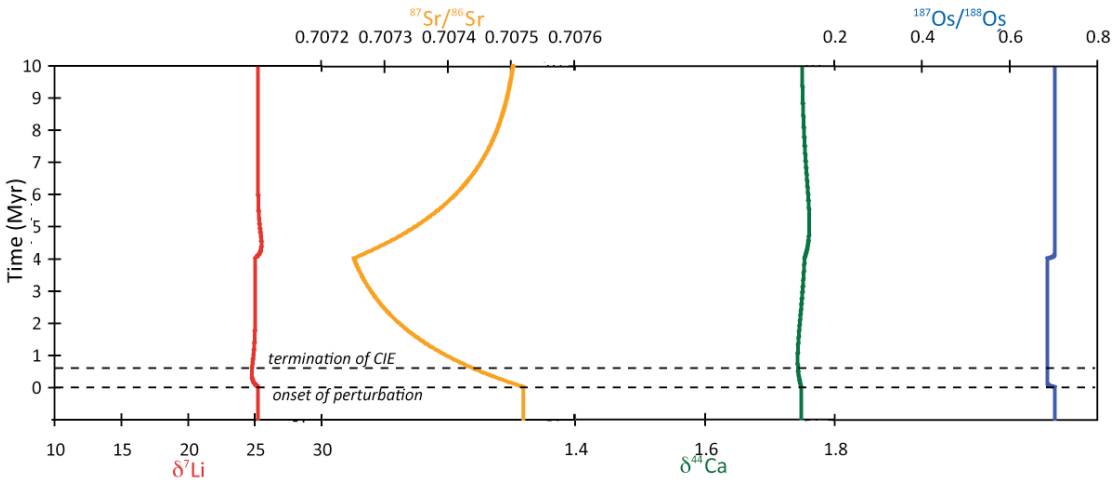

Figure S4. Effect of a 4 Myr 20% hydrothermal flux increase.

Once the hydrothermal flux changes have been accounted for, Li isotopes can be used to constrain the changes in continental weathering. Given that the expanded Eastbourne section shows that seawater δ^7Li had recovered by the end of the carbon isotope excursion, the process that perturbed δ^7Li must have been shorter than ~430 kyr, and probably ~200 kyr, given the need for recovery time. Figure S5A shows the effects on modelled δ^7Li of increasing the river flux by a factor of five for 200 kyr. Equally, it is possible that the river flux stayed constant, and the river δ^7Li decreased, due to a change in weathering intensity[58]. Thus, Figure S5B shows the effect of a 200 kyr decrease in river δ^7Li to a value close to that of continental silicates (0–2‰). Neither process has sufficient effect to perturb seawater δ^7Li to the values observed in the measured carbonate. A combination of the two processes (i.e. an increase in weathering rate and in weathering intensity: Fig. S5C) is still not sufficient to cause the required perturbation. A further issue is the time it takes for a seawater δ^7Li perturbation to recover, given that the modern residence time of Li in the oceans is too high to allow recovery within ~400–500 kyrs. Residence time is determined by the ratio of reservoir size (N_{Li}) to ocean throughput flux, and hence a decrease in

residence time can be caused by a decrease in reservoir size, or an increase in throughput. Given that the Li sink from the oceans is determined in this model by a constant partition coefficient (i.e. reactive to seawater concentration), an increase in the throughput can be achieved by an increase in the input fluxes. Hence, for seawater δ^7Li to recover to pre-excursion values in the observed time interval, either the seawater budget must be reduced (Fig. S4D), or the initial river flux must be increased relative to the present-day flux (Fig S5E).

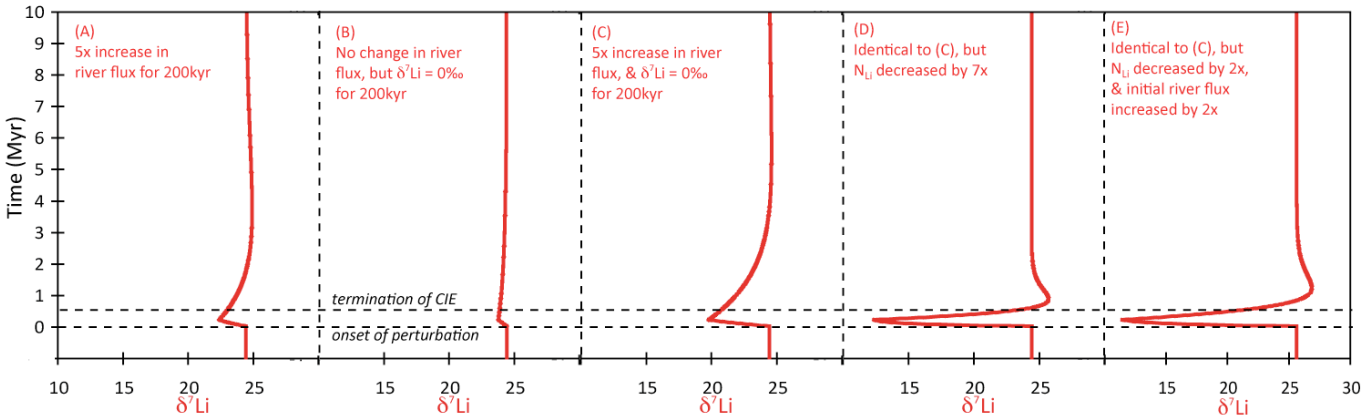

Figure S5. Response of seawater δ^7Li to changes in the riverine flux and isotope ratio.

The effects on the ocean chemistry model of reducing N_{Li} while maintaining a constant throughput flux vs. an increasing input flux while maintaining a constant N_{Li}, are shown in Fig. S6. The mathematical effects of variations in either parameter are similar, but the geological consequences are different, and are discussed below.

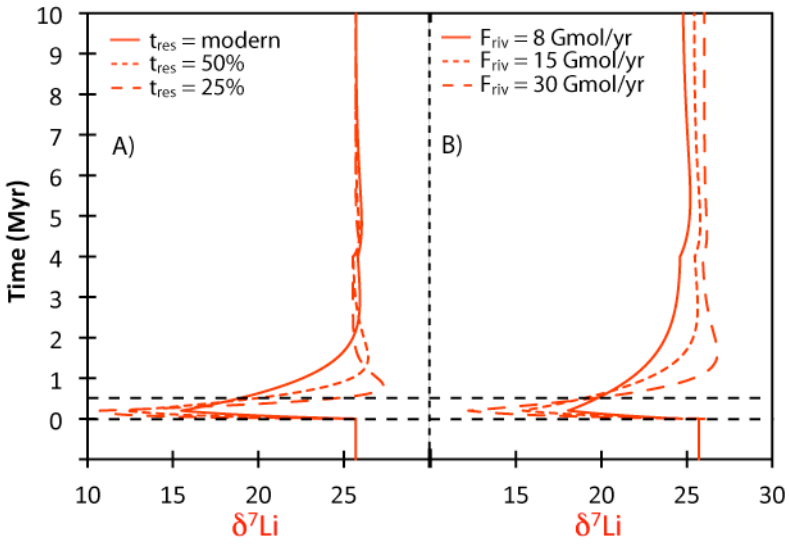

Fig. S6. A) Decrease in ocean reservoir size with constant river flux, resulting in lower ocean residence time and B) increase in river input flux with a constant ocean reservoir size, also resulting in lower ocean residence time (given a constant partition coefficient in the Li sink).

Os isotopes provide a further constraint on the composition of the weathering flux. Turgeon and Creaser 2008 reported a decrease in $^{187}Os/^{188}Os$ to highly unradiogenic values (~0.17) starting slightly before OAE2, and recovering to 0.6 by the end of the carbon isotope excursion. Given that the modern continental weathering flux makes up ~70% of the Os input to the oceans, and its modern $^{187}Os/^{188}Os$ is ~ 1.26, it is not possible to explain OAE2 unradiogenic values using modern fluxes and isotope ratios without increasing the hydrothermal (unradiogenic) flux ~ ×50. However, as shown in Figure S3, such an increase would drive $^{87}Sr/^{86}Sr$ to extremely unradiogenic values. Thus, given that the inference is that seawater $^{187}Os/^{188}Os$ dropped to mantle-like values, the suggestion would be that all the major Os inputs to the ocean had mantle-like compositions (Fig. S7): the "magmatic event" of Turgeon and Creaser 2008[77]. From a mass-balance perspective, this geochemical change could

only occur if a) the weathering flux were radiogenic (i.e. modern) but was insignificant compared with the hydrothermal flux, or b) the weathering flux were also unradiogenic. Given the high temperatures inferred for OAE2[80,81], the former is unlikely. For the latter possibility to be true, the weathering of mantle-derived rocks (e.g. basalts) must have dominated the input flux to the oceans. Massive subaerial volcanism has been proposed during OAE2, linked to the Caribbean or Madagascar Large Igneous Provinces, based on C and Pb isotopes[82]. Such an event would not only provide easily weathered basalt[83,84], but would also release large quantities of CO_2 into the atmosphere, causing global warming, and likely increasing silicate weathering of a variety of substrates. Thus, the observed Os isotope change can be accounted for by an increase in the weathering flux from mantle-derived materials, such as basalt, but clearly cannot be explained by an increase in weathering of continental crust, which is radiogenic.

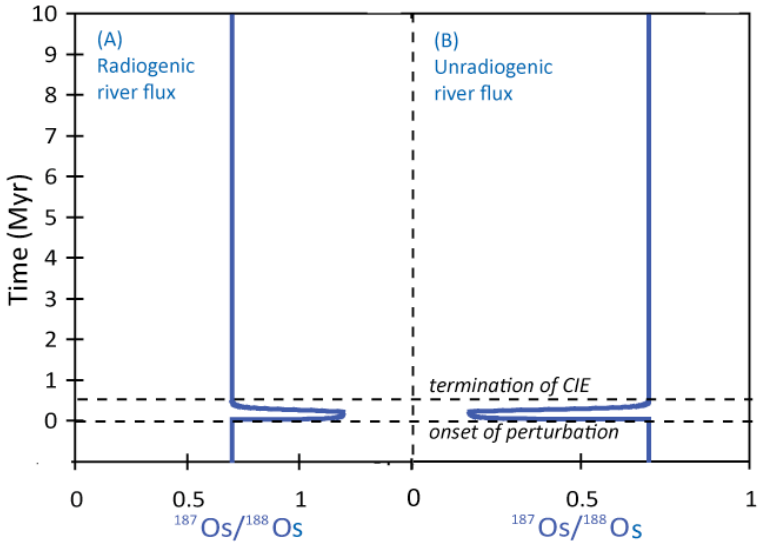

Figure S7. Model results of a radiogenic (modern) vs. unradiogenic Os weathering source.

If submarine or subaerial basalt weathering dominantly accounted for the input of material during the OAE, then the relative proportions of Li, Ca, Sr and Os in the mafic-derived flux would have changed, compared to a continental crust-derived weathering source. Therefore, during the OAE, the relative weathering fluxes are adjusted to be similar to rivers draining modern basaltic environments. In particular, warm basaltic islands with high weathering rates such as the Azores or Réunion are taken to be representative of the OAE weathering regime[85,86]. Less is known about weathering of basaltic terrains for Os, and therefore we use data from Iceland as a source of Os/Sr and Os/Ca ratios (Table S6)[73]. It is important to use river rather than rock elemental ratios, because the elements we are examining have significantly different mobilities in the weathering environment. For example, the Os/Sr of rivers draining basaltic terrains are at the upper limit of those draining continental crust and, in addition, rivers draining fresh basalts have similar Os concentrations to those draining continental crust[60,73].

Molar ratios in basaltic rivers			
	Iceland	Azores	Réunion
Li/Sr	0.8	0.4	0.23
Ca/Sr	1700	220	1000
Os/Sr	500		

Table S6. Approximate average elemental ratios in rivers draining basaltic terrains. Values are from[69,70,73,85-87]. Os/Sr ratios are in nmol/mol; all others in mol/mol.

Hence, an increase in the Li river flux must be combined with increases in the Ca, Sr and Os river fluxes that mimic a mass balance between pre-OAE weathering of continental crust, combined with a significant increase in basaltic weathering (Table S5). Equally, riverine isotope ratios must reflect a similar mass balance[69,73,85,86,88].

However, a weathering flux increase cannot account for all the observed variations in $^{87}Sr/^{86}Sr$, because the Sr isotope excursion would then be of the same duration as the other isotope systems. Hence, an increase in both the weathering and hydrothermal flux is required. Figure S8 illustrates the result of increasing the riverine flux, but maintaining modern fluvial isotope ratios (aside from Li, where δ^7Li is decreased to match a more transport-limited regime), so effectively increasing the weathering of continental crust. While the general observed $^{87}Sr/^{86}Sr$ decrease within 4 Myr can be explained by a 20% increase in hydrothermal flux, weathering of the continental crust clearly drives both Sr and Os isotopes in the wrong (radiogenic) direction.

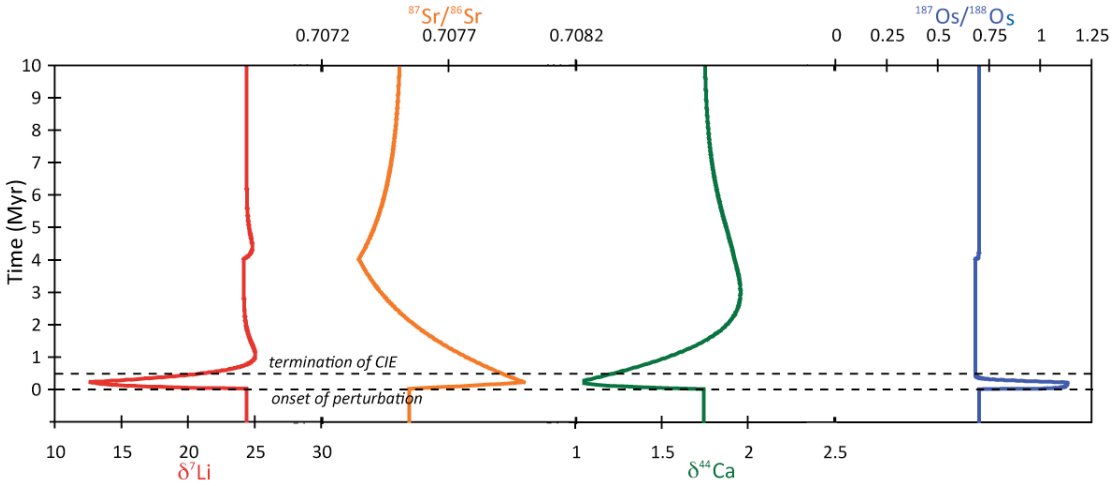

Figure S8. Model results for an increase in the riverine flux 5×, while maintaining modern (continental crust-like) isotope ratios.

Hence, the only realistic approach for explaining the Li, Ca, Sr and Os isotope variations is by invoking a 4Myr 20% increase in the hydrothermal flux, combined with an increase in weathering rates of mafic basalt-like material and an increase in the silicate weathering intensity (Fig. S9). The minimum increase required is ~7× for the Li weathering flux, assuming a modern ocean residence time. However, such a figure is unlikely, given the relatively rapid recovery to pre-excursion values.

Increases in the riverine flux relative to the modern both before and during the excursion would account for the signal, but would also necessitate dissolution of potentially unfeasible amounts of basalt: for the models shown in Fig. S6, ~5.5×10^6 km^3 (~28 km^3/yr) of basalt would need to be dissolved, which is a large fraction of the total LIP eruption during this time (Madagascar ~4.5×10^6 km^3, Caribbean ~4.5×10^6 km^3, phase 2 Ontong-Java ~6×10^6 km^3 [89]).

Hence Figure S9 shows model results of the combined hydrothermal increase, and a 200 kyr pulse of basaltic weathering (where the river flux for the different elements is in proportion to basaltic weathering (Table S5 and S6)) for different ocean elemental reservoirs (i.e. decreasing ocean residence time). The modelled river flux increases during the OAE are tuned to the decreasing residence time, so that while a system with a modern residence time requires a ≥7× increase in the weathering flux, a 50% residence time requires a ≥4× increase, and a 25% residence time a 2–3 times increase. Respectively, this would cause the dissolution of ~2.7, 1.9 and 0.6–1.2 $\times10^6$ km^3 of basalt, approximately 45–60%, 32–42% and 10–27% of individual LIPs during this time[82,89], assuming a basaltic Li concentration of ~7 μg/g (although it should be noted that basalts with [Li] up to 16 μg/g have been reported[86]). It therefore seems most likely that a volume of basalt equivalent to around 10–30% of one of the erupting LIPs was dissolved by this enhanced weathering, and hence that the ocean residence time of Li was reduced during this time. This is likely, if the initial, Late Cretaceous weathering regime was generally characterised by relatively high temperatures, thick soils (transport-limited regime[69,90]) and therefore lower cation supply, as well as faster MOR spreading relative to the present, which could supply more basaltic material for Li uptake during low-temperature alteration of the oceanic

crust (reducing the Li ocean reservoir and hence lowering the residence time). Other studies have also proposed lower residence times for Sr in the late Cretaceous[91]

Given that the silicate weathering rate-weighted average Li concentrations of river waters from basaltic catchments (Iceland[72]) are only ~2 times greater than in continental crust catchments (Mackenzie Basin[68]), it seems likely that total silicate weathering rates during the OAE were approximately 1.5–3 times higher than before the OAE. Hence a 2–3 times increase in the Li river flux is consistent with weathering increases estimated from independent GENIE modelling based on oxygen and sulphur cycles[92]. As discussed in the main text, given that the eruption of Large Igneous Provinces will probably have a significant submarine, as well as subaerial, component, both weathering of basalt in shallow marine and continental environments may have occurred. Both processes would be expected to have similar consequences for ocean chemistry and atmospheric CO_2 sequestration[93].

It is possible to re-create the brief radiogenic Sr isotope spike reported by Frijia and Parente (2008)[91], by increasing the riverine $^{87}Sr/^{86}Sr$ by 0.001 to a more radiogenic composition. It is possible, therefore, that small local variations in the river composition are the reason that this spike has so far only been observed in one section.

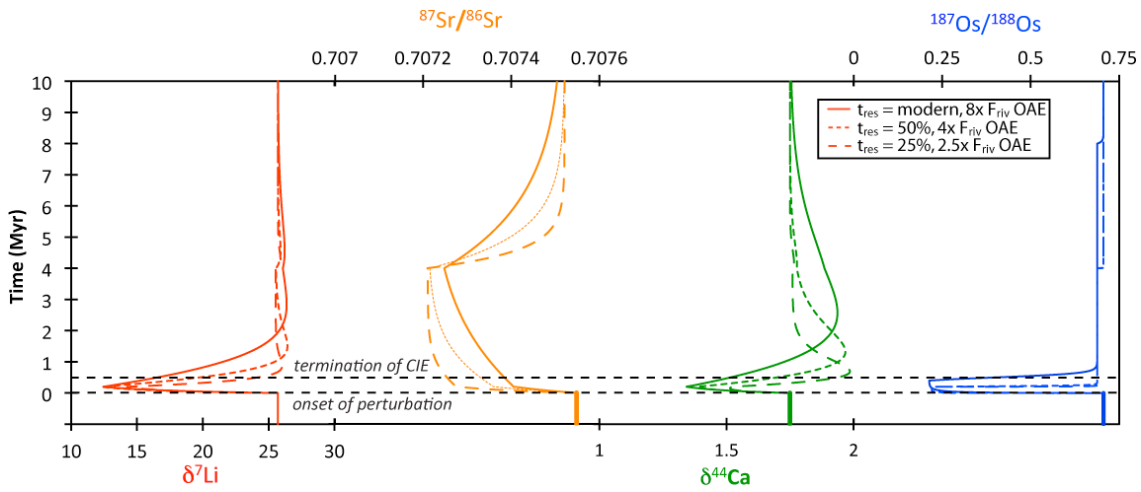

Figure S9. Final combination of parameters (i.e., best fit to observed data: 4 Myr 20% increase in hydrothermal input, combined with increased riverine flux from basaltic weathering). Model lines represent different ocean residence times, with the increase in basalt weathering during the OAE tuned to provide the observed Li isotope excursion. The model results for the other isotope systems reflect the Li isotope model. See text and main article for details.

Given the congruent nature of weathering during the OAE, it is possible to calculate the amounts of basalt dissolution and CO_2 consumption. The amount of basalt dissolution is a simple calculation with parameters given by the weathering model, and uncertainty based on the concentration of the various elements in the basalt. The amount of CO_2 consumed was then calculated based on the theoretical and demonstrably linear relationship between modern silicate weathering rates in global rivers and CO_2 consumption rates, both during weathering of continental crust lithologies[84] and basalts[83]. Given that this relationship holds over greater than two orders of magnitude, and CO_2 consumption is defined by a basic chemical reaction, it is highly likely that this relationship would have held during the Cretaceous.

Li isotope fractionation factors in calcite

A Li isotope fractionation factor is thought to take place during the precipitation or secretion of carbonate. While a range of isotopic offsets has been reported, both from experimentally grown calcite, as well as from foraminifera and corals, this range is significantly smaller than the δ^7Li variations reported in this study. Thus Marriott et al. (2004a,b) showed that δ^7Li in inorganic calcite grown from seawater, as well as in benthic foraminifera and corals, is fractionated by 3–5‰,

irrespective of changes in temperature, salinity or Li/Ca. Published Li isotope fractionation in planktonic foraminifera shows slightly more variable offsets: Hall and Chan (2004) show that average *O. universa* is ~1.3‰ lighter than seawater, although high uncertainty on these measurements means that fractionation could vary between -2.4 and +4.3‰[94]. Although species-specific isotope fractionation for planktonic foraminifera has been reported [63], the amount of δ^7Li offset caused by biomineralisation was not greater than 0–4‰, although, again, analytical uncertainty was relatively high in this study (±1‰). Equally, Misra and Froehlich (2009, 2012) report modern foraminiferal δ^7Li up to 4‰ lighter than seawater[58,95]. Finally, studies of shallow- and deep-water corals show that they are isotopically homogenous, and δ^7Li values are not affected by changes in temperature, pH and pCO_2[96]. Combined, these studies suggest that there is a small Li isotope offset during calcification, and that carbonates tend to precipitate isotopically lighter than seawater. Thus, given that foraminifera as old as 70 Myr are thought to be a reliable and faithful reservoir of seawater δ^7Li[58,97], we are confident that bulk carbonates are also useful reservoirs of seawater δ^7Li. The isotopic fractionation factors are small compared to the variability reported in this study, given a fractionation factor of 3–5‰. We apply a fractionation factor of 5‰ to our models, because this gives a minimum estimate in weathering variability (or other inputs).

More importantly for this study, while Li/Ca ratios in calcite have been shown to be dependent on temperature and salinity (with opposing directions of fractionation), data suggest that the fractionation imposed on Li isotopes during uptake into inorganic and biogenic calcite remains relatively constant and, critically, is independent of temperature or salinity[94-96,98-100]. Hence, our bulk carbonate δ^7Li record is also likely not influenced by changes in these parameters.

Supplementary References

51 Tessier, A., Campbell, P. G. C. & Bisson, M. Sequential Extraction Procedure for the Speciation of Particulate Trace Metals. *Analytical Chemistry* **51**, 844-851 (1979).

52 Pearce, M. A., Jarvis, I. & Tocher, B. A. The Cenomanian–Turonian boundary event, OAE2 and palaeoenvironmental change in epicontinental seas: New insights from the dinocyst and geochemical records. *Palaeogeography, Palaeoclimatology, Palaeoecology* **280**, 207–234 (2009).

53 Pogge von Strandmann, P. A. E. *et al.* Variations of Li and Mg isotope ratios in bulk chondrites and mantle xenoliths. *Geochim. Cosmochim. Acta* **75**, 5247–5268 (2011).

54 Tomascak, P. B. in *Geochemistry of Non-Traditional Stable Isotopes* Vol. 55 *Reviews in Mineralogy & Geochemistry* (eds C. M. Johnson, B. L. Beard, & F. Albarède) 153–195 (2004).

55 Flesch, G. D., Anderson, A. R. & Svec, H. J. A secondary isotopic standard for 6Li/7Li determinations. *Int. J. Mass Spectrom. Ion Process.* **12**, 265–272 (1973).

56 Chan, L. H., Edmond, J. M. & Thompson, G. A lithium isotope study of hot springs and metabasalts from mid-ocean ridge hydrothermal systems. *Journal of Geophysical Research* **98**, 9653-9659 (1993).

57 Huh, Y., Chan, L. H., Zhang, L. & Edmond, J. M. Lithium and its isotopes in major world rivers: Implications for weathering and the oceanic budget. *Geochim. Cosmochim. Acta* **62**, 2039–2051 (1998).

58 Misra, S. & Froelich, P. N. Lithium Isotope History of Cenozoic Seawater: Changes in Silicate Weathering and Reverse Weathering. *Science* **335**, 818–823 (2012).

59 Sharma, M., Papanastassiou, D. A. & Wasserburg, G. J. The concentration and isotopic composition of osmium in the oceans. *Geochim. Cosmochim. Acta* **61**, 3287-3299 (1997).

60 Levasseur, S., Birck, J. L. & Allègre, C. J. The osmium riverine flux and the oceanic mass balance of osmium. *Earth Planet. Sci. Lett.* **174**, 7–23 (1999).

61 Palmer, M. R. & Edmond, J. M. The Strontium Isotope Budget of the Modern Ocean. *Earth Planet. Sci. Lett.* **92**, 11–26 (1989).

62 Vance, D., Teagle, D. A. H. & Foster, G. L. Variable Quaternary chemical weathering fluxes and imbalances in marine geochemical budgets. *Nature* **458**, 493–496 (2009).

63 Hathorne, E. C. & James, R. H. Temporal record of lithium in seawater: a tracer for silicate weathering? *Earth Planet. Sci. Lett.* **246**, 393–406 (2006).

64 Sharma, M. & Wasserburg, G. J. Osmium in the rivers. *Geochim. Cosmochim. Acta* **61**, 5411–5416 (1997).

65 Blättler, C. L., Jenkyns, H. C., Reynard, L. M. & Henderson, G. M. Significant increases in global weathering during Oceanic Anoxic Events 1a and 2 indicated by calcium isotopes. *Earth Planet. Sci. Lett.* **309**, 77–88 (2011).

66 Berner, R. A. GEOCARB II: A revised model of atmospheric CO2 over Phanerozoic time. *Am. J. Sci.* **294**, 56–91 (1994).

67 Kisakürek, B., James, R. H. & Harris, N. B. W. Li and δ^7Li in Himalayan rivers: Proxies for silicate weathering? *Earth Planet. Sci. Lett.* **237**, 387–401 (2005).
68 Millot, R., Vigier, N. & Gaillardet, J. Behaviour of lithium and its isotopes during weathering in the Mackenzie Basin, Canada. *Geochim. Cosmochim. Acta* **74**, 3897–3912 (2010).
69 Pogge von Strandmann, P. A. E., Burton, K. W., James, R. H., van Calsteren, P. & Gislason, S. R. Assessing the role of climate on uranium and lithium isotope behaviour in rivers draining a basaltic terrain. *Chem. Geol.* **270**, 227–239 (2010).
70 Pogge von Strandmann, P. A. E. *et al.* Riverine behaviour of uranium and lithium isotopes in an actively glaciated basaltic terrain. *Earth Planet. Sci. Lett.* **251**, 134–147 (2006).
71 Pogge von Strandmann, P. A. E. *et al.* Lithium, magnesium and silicon isotope behaviour accompanying weathering in a basaltic soil and pore water profile in Iceland. *Earth Planet. Sci. Lett.* **339–340**, 11–23 (2012).
72 Vigier, N., Gislason, S. R., Burton, K. W., Millot, R. & Mokadem, F. The relationship between riverine lithium isotope composition and silicate weathering rates in Iceland. *Earth Planet. Sci. Lett.* **287**, 434–441 (2009).
73 Gannoun, A. *et al.* The influence of weathering process on riverine osmium isotopes in a basaltic terrain. *Earth Planet. Sci. Lett.* **243**, 732-748 (2006).
74 Allegre, C. J. *et al.* The fundamental role of island arc weathering in the oceanic Sr isotope budget. *Earth Planet. Sci. Lett.* **292**, 51-56, doi:10.1016/j.epsl.2010.01.019 (2010).
75 Taylor, A. S. & Lasaga, A. C. The role of basalt weathering in the Sr isotope budget of the oceans. *Chem. Geol.* **161**, 199-214 (1999).
76 Veizer, J. *et al.* Sr-87/Sr-86, delta C-13 and delta O-18 evolution of Phanerozoic seawater. *Chem. Geol.* **161**, 59–88 (1999).
77 Turgeon, S. C. & Creaser, R. A. Cretaceous oceanic anoxic event 2 triggered by a massive magmatic episode. *Nature* **454**, 323–327 (2008).
78 Farkaš, J. *et al.* Calcium isotope record of Phanerozoic oceans: Implications for chemical evolution of seawater and its causative mechanisms. *Geochim. Cosmochim. Acta* **71**, 5117–5134, doi:10.1016/j.gca.2007.09.004 (2007).
79 Jenkyns, H. C. Geochemistry of oceanic anoxic events. *Geochem. Geophys. Geosyst.* **11**, Q03004, doi:10.1029/2009GC002788 (2010).
80 Forster, A., Schouten, S., Moriya, K., Wilson, P. A. & Sinninghe Damsté, J. S. Tropical warming and intermittent cooling during the Cenomanian/Turonian oceanic anoxic event 2: Sea surface temperature records from the equatorial Atlantic. *Paleoceanography* **22**, PA1219, doi:10.1029/2006PA001349 (2007).
81 Sinninghe Damsté, J. S., van Bentum, E. C., Reichart, G. J., Pross, J. & Schouten, S. A CO_2 decrease-driven cooling and increased latitudinal temperature gradient during the mid-Cretaceous Oceanic Anoxic Event 2. *Earth Planet. Sci. Lett.* **293**, 97–103, doi:10.1016/j.epsl.2010.02.027 (2010).
82 Kuroda, J. *et al.* Contemporaneous massive subaerial volcanism and late Cretaceous Oceanic Anoxic Event 2. *Earth Planet. Sci. Lett.* **256**, 211–223 (2007).
83 Dessert, C., Dupre, B., Gaillardet, J., Francois, L. M. & Allegre, C. J. Basalt weathering laws and the impact of basalt weathering on the global carbon cycle. *Chem. Geol.* **202**, 257–273 (2003).

84 Gaillardet, J., Dupre, B., Louvat, P. & Allegre, C. J. Global silicate weathering and CO_2 consumption rates deduced from the chemistry of large rivers. *Chem. Geol.* **159**, 3-30 (1999).
85 Louvat, P. & Allegre, C. J. Present denudation rates on the island of Reunion determined by river geochemistry: Basalt weathering and mass budget between chemical and mechanical erosions. *Geochim. Cosmochim. Acta* **61**, 3645-3669 (1997).
86 Louvat, P. & Allegre, C. J. Riverine erosion rates on Sao Miguel volcanic island, Azores archipelago. *Chem. Geol.* **148**, 177-200 (1998).
87 Gíslason, S. R., Arnorsson, S. & Armannsson, H. Chemical weathering of basalt in southwest Iceland: Effects of runoff, age of rocks and vegetative/glacial cover. *Am. J. Sci.* **296**, 837–907 (1996).
88 Tipper, E. T., Galy, A. & Bickle, M. J. Riverine evidence for a fractionated reservoir of Ca and Mg on the continents: Implications for the oceanic Ca cycle. *Earth Planet. Sci. Lett.* **247**, 267-279 (2006).
89 Courtillot, V. E. & Renne, P. R. On the ages of flood basalt events. *C. R. Geosci.* **335**, 113–140 (2003).
90 West, A. J., Galy, A. & Bickle, M. Tectonic and climatic controls on silicate weathering. *Earth Planet. Sci. Lett.* **235**, 211–228 (2005).
91 Frijia, G. & Parente, M. Strontium isotope stratigraphy in the upper Cenomanian shallow-water carbonates of the southern Apennines: Short-term perturbations of marine $^{87}Sr/^{86}Sr$ during the oceanic anoxic event 2. *Palaeogeography, Palaeoclimatology, Palaeoecology* **261**, 15–29 (2008).
92 Monteiro, F. M., Pancost, R. D., Ridgwell, A. & Donnadieu, Y. Nutrients as the dominant control on the spread of anoxia and euxinia across the Cenomanian-Turonian oceanic anoxic event (OAE2): Model-data comparison. *Paleoceanography* **27, PA4209**, doi:10.1029/2012PA002351 (2012).
93 Gíslason, S. R., Oelkers, E. & Snorrason, A. Role of river-suspended material in the global carbon cycle. *Geology* **34**, 49–52 (2006).
94 Hall, J. M., Chan, L. H., McDonough, W. F. & Turekian, K. K. Determination of the lithium isotopic composition of planktic foraminifera and its application as a paleo-seawater proxy. *Marine Geology* **217**, 255–265, doi:10.1016/j.margeo.2004.11.015 (2005).
95 Misra, S. & Froelich, P. N. Measurement of lithium isotope ratios by quadrupole-ICP-MS: application to seawater and natural carbonates. *J. Anal. At. Spectrom.* **24**, 1524-1533, doi:10.1039/b907122a (2009).
96 Rollion-Bard, C. *et al.* Effect of environmental conditions and skeletal ultrastructure on the Li isotopic composition of scleractinian corals. *Earth Planet. Sci. Lett.* **286**, 63–70 (2009).
97 Burton, K. W. & Vigier, N. in *Handbook of Environmental Isotope Geochemistry* (ed M. Baskaran) 41–59 (Springer, 2011).
98 Hall, J. M. & Chan, L. H. Li/Ca in multiple species of benthic and planktonic foraminifera: Thermocline, latitudinal, and glacial-interglacial variation. *Geochim. Cosmochim. Acta* **68**, 529–545, doi:10.1016/s0016-7037(00)00451-4 (2004).
99 Marriott, C. S., Henderson, G. M., Belshaw, N. S. & Tudhope, A. W. Temperature dependence of δ^7Li, $\delta^{44}Ca$ and Li/Ca during growth of calcium carbonate. *Earth Planet. Sci. Lett.* **222**, 615–624 (2004).

100 Marriott, C. S., Henderson, G. M., Crompton, R., Staubwasser, M. & Shaw, S. Effect of mineralogy, salinity, and temperature on Li/Ca and Li isotope composition of calcium carbonate. *Chem. Geol.* **212**, 5–15 (2004).